Received 30 January 2019; revised 29 May 2019, 11 June 2019, and 26 June 2019; accepted 7 July 2019. Date of publication 9 July 2019; date of current version 1 August 2019. The review of this paper was arranged by Editor K. Shenai.

Digital Object Identifier 10.1109/JEDS.2019.2927608

Precise Extraction of Dynamic R_{dson} Under High Frequency and High Voltage by a Double-Diode-Isolation Method

JIANMING LEI, RUI WANG, GUO YANG, JIN WANG, FULONG JIANG, DUNJUN CHEN, HAI LU, RONG ZHANG, AND YOUDOU ZHENG

Key Laboratory of Advanced Photonic and Electronic Materials, School of Electronic Science and Engineering, Nanjing University, Nanjing 210093, China

CORRESPONDING AUTHOR: D. CHEN (e-mail: djchen@nju.edu.cn)

This work was supported in part by the National Key Research and Development Program of China under Grant 2017YFB0402900, in part by NSF of China under Grant 61634002 and Grant 61474060, and in part by the Key Project of Jiangsu Province, China, under Grant BE2016174.

ABSTRACT A double-diode-isolation method with low parasitic capacitance devices and reverse clamping is proposed to accurately extract the high-frequency and high-voltage dynamic on-resistance (R_{dson}) of AlGaN/GaN high electron mobility transistor (HEMT) power devices. The response time required for the drain voltage to drop back to the on-voltage of this testing circuit can reach 100 ns, and the forward voltage drop of the isolation diode is monitored in real time using low-voltage probes. A low value constant current source is built to power the testing circuit at only several mA to avoid additional self-heating effect. With these improvements, we can obtain a test frequency of more than 1 MHz, a test voltage of more than 600 V and an accuracy of higher than 97.8% for the extraction of dynamic R_{dson}.

INDEX TERMS AlGaN/GaN HEMT device, dynamic on-resistance, parasitic capacitance, trapping effect.

I. INTRODUCTION

AlGaN/GaN high electron mobility transistor (HEMT) power electronic devices have several merits due to their wide bandgap energy, high electron mobility and strong polarization [1]–[3]. However, the high off-state drain voltage (V_{ds_off}) leads to trapping processes [4]–[5], so the dynamic on-resistance (R_{dson}) may be several times larger than DC R_{dson} and becomes the major factor in the power loss in AlGaN/GaN HEMTs [6]–[7].

The voltage swing at the drain side is very large, ranging from several millivolts in the on-state to hundreds of volts in the off-state [8]–[9]. To extract the dynamic R_{dson} precisely, several state-of-the-art circuits were proposed [10]–[15]. Lu *et al.* used a voltage clamping by MOSFETs (metal-oxide semiconductor field-effect transistors), as shown in Fig. 1(a), and Badawi *et al.* used a voltage isolation by SiC diodes, as shown in Fig. 1(b). The MOSFET and SiC diode used in these two methods have large parasitic capacitance while voltage stress is below 10 V, and this capacitance will greatly affect the frequency response of the testing circuit, so their testing frequency is below 250 kHz. In addition, the MOSFET in [10] keeps operating in a linear conducting state. This behavior will introduce a leakage current leading to a voltage drop across the MOSFET. Whereas the test circuit in [11] is supplied by an energy storage capacitor, thus, the forward current of the isolation diode is not constant, and the forward voltage drop of the isolation diode is variable. Obviously, these voltage drops in [10] and [11] will reduce the extraction accuracy of dynamic R_{dson}. Gelagaev and Everts *et al.* used a cascade current mirror, as shown in Fig. 1(c), and carried out the testing below the conditions of 2 MHz f_s and 300 V V_{ds_off} [12]–[15]. However, the currents in the two branches are not in exactly 1:1, and this current ratio is slightly affected by the high dV/dt of the point A. In addition, the large currents they used (about 80 mA) will bring temperature problem as well as different voltage drops between D_A and D_B. This result will affect the test accuracy of the dynamic R_{dson}. Also, a freewheeling diode has not been employed to cause reverse clamping, which also greatly affects the frequency response of the testing circuit.

TABLE 1. The comparison with our work and works in [10]–[15].

Subject	*Isolation Method*	*Power Supply*	*Supply Current*	*Measurement Error*	*Reverse Clamping*	*Parasitic Capacitance*
Ref. 10	Single MOSFET	Voltage Source	Large	Not Considered	Yes	Very Large
Ref. 11	Single SiC Diode	Voltage Source	Large	Not Considered	Yes	Large
Ref. 12-15	Single Diode in High-side and Low-side	Mirror Current Source	Medium	Not Considered	No	Small But Not Specified Its Impact
Our's	Double Diodes in Series in High-side Only	Constant Current Source	Small	Considered	Yes	Smallest

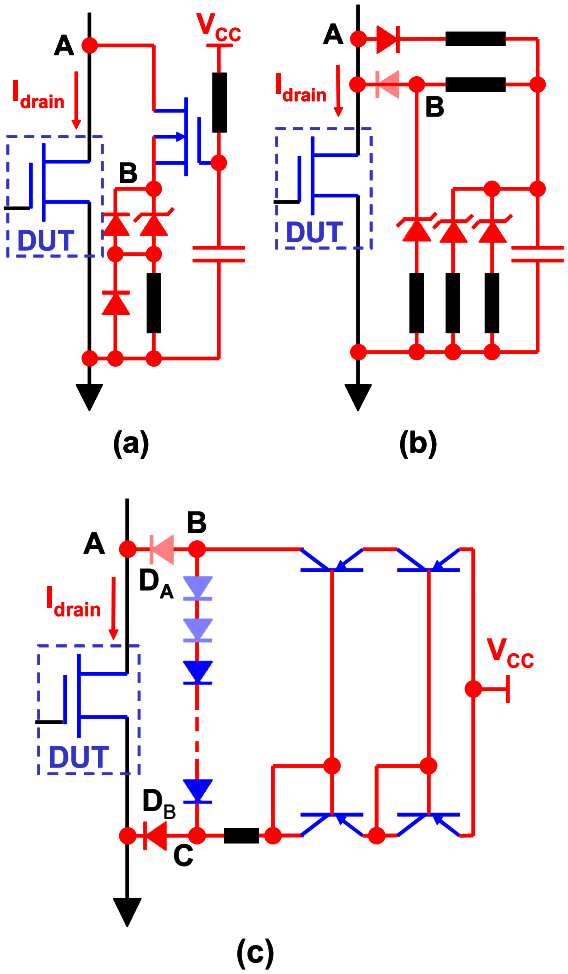

FIGURE 1. Dynamic R_{dson} extraction circuit in [10] (a), [11] (b) and [12]–[15] (c).

With the increase of V_{ds_off}, the parasitic capacitance of the functional devices (including the isolation diodes and reverse clamping diodes) will become larger and the impact of the freewheeling diode on the frequency response will become more obvious. Further, none of these methods monitors the voltage drop of the isolation device in real time, or discusses the relationships between dynamic R_{dson}, f_s and the duty cycle (D).

In this work, a new method is proposed for extracting the dynamic R_{dson} of AlGaN/GaN HEMT power devices operated at high frequency and high drain voltage. First, double isolation diodes in series at high-side and freewheeling diodes with high voltage and low parasitic capacitance are employed, where the series combination of the double isolation diodes can further reduce the parasitic capacitance and hence improve the frequency response of the test circuit. Then, the forward voltage drop of one isolation diode (V_F) is measured in real time, and a high precision and low value constant current source is used to improve the extraction accuracy of dynamic R_{dson} and avoid additional self-heating effect. The detailed comparison with our work and previous works in [10]–[15] is shown in Table 1. Finally, the accuracy of this extraction is quantified by a statistical method.

II. DYNAMIC RDSON EXTRACTION METHOD

Fig. 2 shows the extraction circuit and the printed circuit board (PCB) for the dynamic R_{dson}. In this circuit, we used D_1 and D_2 as the double isolation diodes. D_1 isolation makes it possible to test the V_F of D_2 at low-voltage in real time. This approach allows an accurate estimate of the V_F of D_1 having the same forward current. D_3 and ZD_1 are freewheeling diodes with ZD_1 also acting as a positive clamping diode. These diodes, having very low parasitic capacitance, are specially chosen to improve the high-frequency response. Constant current I_1 is set by a 5 V constant voltage source (VCC) and a constant current diode of 3 mA or lower. Thus, D_1 and D_2 are selected as UF4007 (1 A/1000 V) which have a parasitic capacitance of about 40 pF in the voltage stress of less than 10 V, and a reverse recovery time (t_{rr}) of about 100 ns. D_3 and ZD_1 are selected as small-signal diode 1N4148 (150 mA/100 V) and general Zener (5 V/0.5 W) which have parasitic capacitance below 0.9 pF and t_{rr} less than 5 ns. Functional devices with lower parasitic capacitance and faster t_{rr} are required for higher frequency responses. 2 KΩ R_t provides a small load for I_1, while R_t and 2 Ω R_1, R_2 are used to suppress the voltage spike. The E-mode AlGaN/GaN HEMT device GS66502B from GaN Systems Inc. (650 V/7.5 A/200 mΩ) is driven by a driver Si8271 from Silicon Labs using a square-wave as signal input.

The dynamic R_{dson} of the AlGaN/GaN HEMT can be tested using the above testing circuit, and the test results are

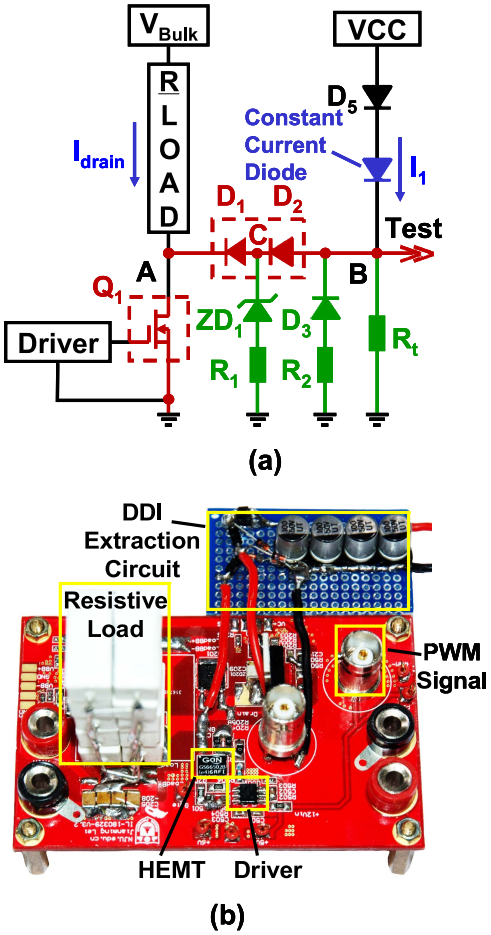

FIGURE 2. Equivalent dynamic R_{dson} extraction circuit (a) and PCB photo (b).

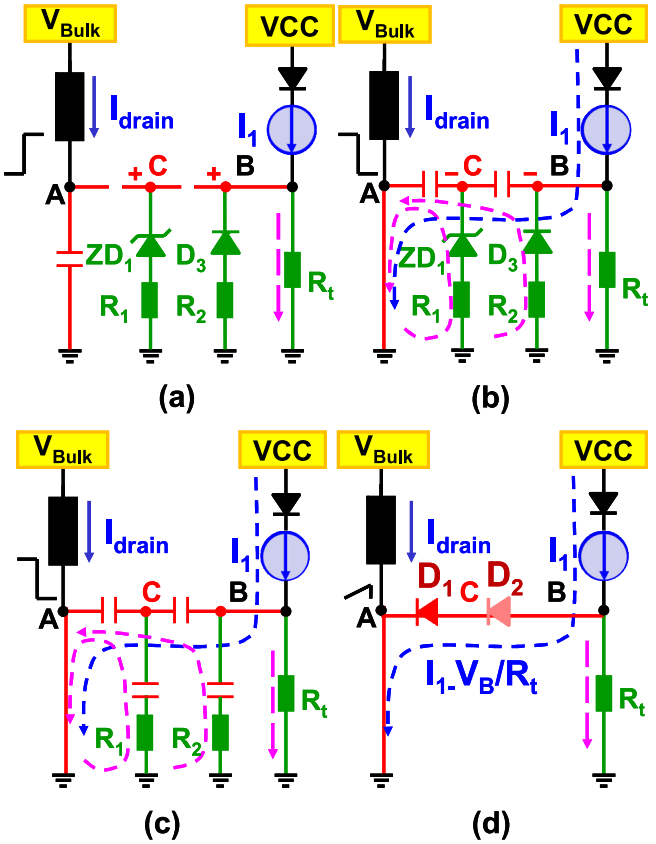

FIGURE 3. Operating processes of dynamic R_{dson} test circuit.

given by

$$R_{dson} = \left(\bar{V}_{\mathrm{B}} - 2\bar{V}_{\mathrm{F\_D2}}\right)/\left(I_{\mathrm{drain}} + I_1 - \bar{V}_{\mathrm{B}}/R_{\mathrm{t}}\right) \qquad (1)$$

where $\overline{V_B}$, $\overline{V}_{F\_D2}$ and $\bar{I}_{drain}$, $\bar{I}_{D2}$, I_1 are the voltage at point B, the forward voltage of D_2, and the current flowing through a resistive load and D_2, and the current of the constant current supply, respectively. As shown in Fig. 3(d), the numerator on the right-hand side of the Eq. (1) is the device drain voltage which can be obtained by testing V_B and V_{F_D2}, assuming that the forward voltage of D_1 (V_{F_D1}) is equal to V_{F_D2}. Similarly, the denominator on the right-hand side of the Eq. (1) is the device channel current which is the sum of the tested I_{drain} and the branch current of I_1 after deducting the current flowing through the R_t.

To further address the important role of the functional devices and their parasitic capacitors, we divide the switching processes into four stages, as shown in Fig. 3. The I_{drain}, V_{drain} and V_B are tested by a current probe (TCP0020), a high-voltage differential probe (THDP0200) and a low-voltage probe with 1:1 attenuation (P2221), respectively, and displayed on an oscilloscope (MDO3104). The V_{F_D2} of D_2 is tested by a low-voltage differential probe with 1:1 attenuation (TIVH02). In particular, the 1:1 attenuation probe will not amplify the background noise when measuring the signal, and can extract the V_B more accurately.

Fig. 3(a) shows the test circuit in off-state, where D_1 and D_2 are switched off. The potential of point C (V_C) is clamped by ZD_1, and V_B is at a low voltage with the value of less than 15 V. Fig. 3(b) shows the test circuit in turn-on transition, and the V_{drain} decreases to an on-state voltage from V_{ds_off} with high dV/dt. Both V_C and V_B become negative because of the parasitic capacitors, and these voltages are clamped by the freewheeling diodes ZD_1 and D_3. Then, the parasitic capacitors are charged by I_1 and the freewheeling currents. If the parasitic capacitance of the isolation device reaches 450 pF, the frequency response will be lower than 100 kHz under $I_1 = 3$ mA and 50% duty cycle conditions, as plotted in Fig. 4(a), where the frequency response is associated with the response time required for the drain voltage drop back to the on-voltage of this testing circuit.

If the freewheeling diodes of ZD_1 and D_3 are removed, the frequency response will exhibit a further drop to below 25 kHz, as shown in Fig. 4(b). If the low parasitic capacitance functional devices mentioned above are used, the frequency response will be higher than 5 MHz with below 100 V V_{ds_off}, as shown in Fig. 4(c). It can be deduced that the test circuit can achieve around 3 MHz frequency

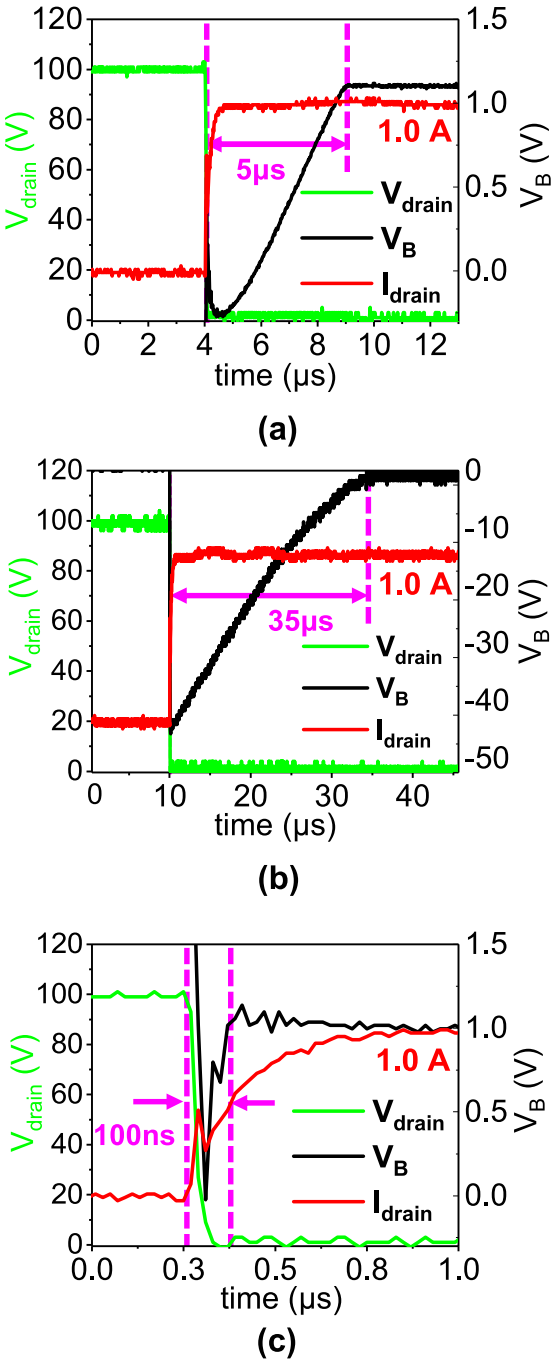

FIGURE 4. Frequency response of test circuit with 450 pF functional devices (a), and (b) after removing the freewheeling diodes from (a), and (c) with our functional devices.

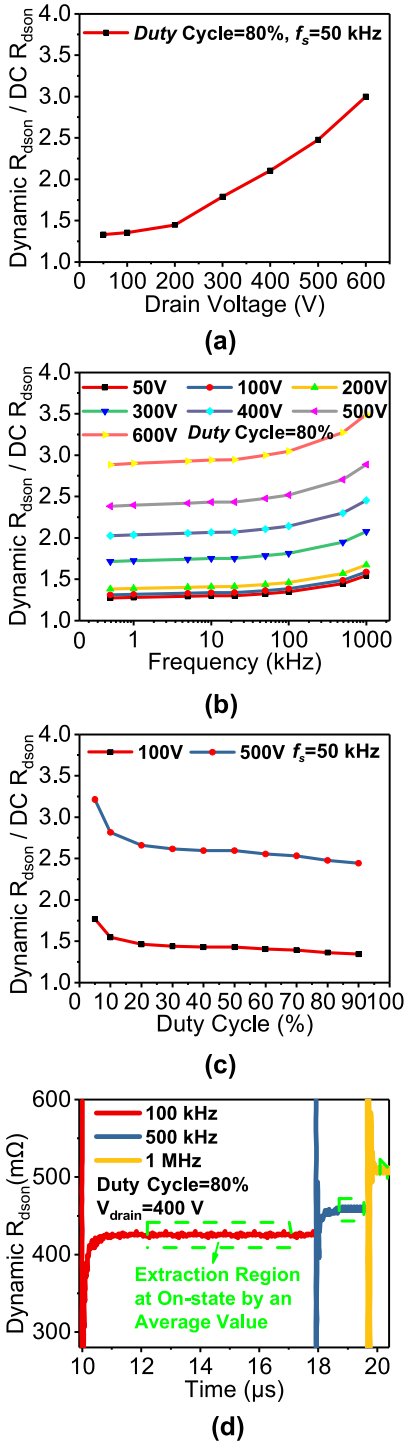

FIGURE 5. The relationship between dynamic R_{dson} and off-state drain voltage (a), operating frequency (b), and duty cycle (c), and diagram of dynamic R_{dson} extraction process (d).

responses under 600 V V_{ds_off} according to a 10 V/ns dV/dt of the HEMT device. From Fig. 3, we can conclude that the parasitic capacitance of these functional devices and the freewheeling diodes have major effects on the frequency response of this extraction circuit.

Fig. 3(c) shows the test circuit still in the turn-on transition, where the ZD_1 and D_3 are blocked when node C and B are charged to a certain voltage. The parasitic capacitors of ZD_1 and D_3 are involved in the charging by I_1 and freewheeling currents. Then D_1 and D_2 are completely forward conducting, and the R_{dson} of the AlGaN/GaN HEMT device can be tested, as shown in Fig. 3(d).

III. EXPERIMENTAL VERIFICATION AND DISCUSSION

Comparative test results of dynamic R_{dson} with a resistive load are shown in Fig. 5 at various values of V_{ds_off}, f_s,

and D, respectively. The dynamic R_{dson} extraction process is illustrated in Fig. 5(d), the conductive voltage and current are measured at on-state of the device with average values in a stable region. As shown in Fig. 5(a), it can be clearly seen that the tested dynamic R_{dson} becomes larger as V_{ds_off} increases. Actually, when the drain voltage is larger than 10 V, the problem of dynamic R_{dson} increase will occur. That means the dynamic R_{dson} is voltage-dependent. Fig. 5(b) and Fig. 5(c) show the relationships between the dynamic R_{dson} and the f_s and D. The tested dynamic R_{dson} increases as the f_s increases or the D decreases. The f_s and D determine the on-state and off-state time, indicating that the dynamic R_{dson} is also determined by the ON and OFF time of the high electric field applied at drain terminal of HEMT. From Fig. 5, the tested dynamic R_{dson} under conditions of 50 kHz f_s, 80% D and 500 V V_{ds_off} is found to be approximately 3 times bigger than DC R_{dson}. Therefore, we can conclude that large drain voltage (> 10 V) is the major reason for the increase in dynamic R_{dson}, while small on-state time and large off-state time is the minor reason. As is well-known, the high electric field introduced by the high drain voltage will lead to the trapping effect of an HEMT device, and the time required for electron trapping is several nanoseconds, the electron detrapping time is several seconds. Therefore, the longer the high drain voltage is applied, the more trapped electrons accumulated, and the larger the dynamic R_{dson} becomes. This is consistent with our test results, and we should pay great attention to the dynamic R_{dson} which becomes the major factor in the power loss of the HEMT device.

IV. QUANTIFYING THE EXTRACTION ACCURACY

We further investigated the accuracy of the dynamic R_{dson} that can be quantified by the absolute errors [16]. We classified the errors into two categories according to their effect on accuracy. The I_1 in Eq. (1) can be ignored, because it is far smaller than I_{drain}. Then, the first kind of absolute error (ΔR_{dson_1}), resulted from the discrepancy between measurement value and real value, can be depicted based on (1) by [17]

$$\Delta R_{dson\_1} \approx \left|\frac{\partial R_{dson}}{\partial \overline{V_B}}\right|\Delta\overline{V_B} + \left|\frac{\partial R_{dson}}{\partial \overline{V}_{F\_D2}}\right|\Delta\overline{V}_{F\_D2} + \left|\frac{\partial R_{dson}}{\partial \bar{I}_{drain}}\right|\Delta\bar{I}_{drain} \tag{2}$$

$$\Delta R_{dson\_1} = \frac{\Delta\overline{V_B}}{\bar{I}_{drain}} + \frac{2\Delta\overline{V}_{F\_D2}}{\bar{I}_{drain}} + \frac{(\overline{V_B} - 2\overline{V}_{F\_D2})\Delta\bar{I}_{drain}}{\bar{I}^2_{drain}} \tag{3}$$

where delta variables denote the test errors (the discrepancy between test value and real value) of corresponding variables. At a temperature of 300 K, the low-voltage test error is obtained by testing a calibrated voltage signal at 50 kHz f_s using 1:1 low voltage probes, and this error is found no more than 4 mV in the range of 0.2-2 V. Thus, the test errors of V_B ($\Delta\overline{V_B}$) and V_{F_D2} ($\Delta\overline{V}_{F\_D2}$) are set to 4 mV. $\overline{V_B} - 2\overline{V}_{F\_D2}$ is tested at 1 A $\bar{I}_{drain}$ under the conditions of 50 kHz f_s, 80% D and 100 V V_{ds_off} and then set to 260 mV. Similarly, the current test error is obtained by testing a calibrated current signal at 50 kHz f_s, and this error is found to be no more than 10% of testing current in the range of 1-5 A. Thus, $\Delta\bar{I}_{drain}$ is set to 10 mA in the condition of 1 A $\bar{I}_{drain}$. Then, the first absolute error of dynamic R_{dson} should be

$$\Delta R_{dson\_1} = (3 \cdot 0.004 + 0.26 \cdot 0.01)/1 = 14.6\ m\Omega$$

The second kind of absolute error (ΔR_{dson_2}) is then the difference of the forward voltage drop of D_1 and D_2 (V_{F_D1} and V_{F_D2}) by [15]

$$\Delta R_{dson\_2} \approx \frac{\left|V_{F\_D1} - V_{F\_D2}\right|}{\bar{I}_{drain}} \approx \frac{nkT}{q\bar{I}_{drain}} \ln\left(1 + \frac{\Delta I_1}{I_1}\right) \approx \frac{nkT}{q\bar{I}_{drain}} \frac{\Delta I_1}{I_1} \tag{4}$$

where, at a temperature of 300 K and 3 mA I_1, the error of I_1 (ΔI_1) is set to 0.1 mA according the maximum accuracy of the device, and the emission coefficient (n) of UF4007 is set to 19.3. When $\bar{I}_{drain}$ is 5 A, (4) can be simplified into

$$\Delta R_{dson\_2} = \frac{19.3 \cdot 1.38065 \cdot 10^{-23} \cdot 300}{1.602 \cdot 10^{-19} \cdot 1} \frac{0.1}{3} \approx 16.6\ m\Omega$$

Thus, according to the principle of the statistical scenario (root sum of squares), the total absolute error of dynamic R_{dson} (ΔR_{dson}) with the above conditions should be [18]

$$\Delta R_{dson} = \sqrt{\Delta R^2_{dson\_1} + \Delta R^2_{dson\_2}} \approx 22.1\ m\Omega$$

To further improve the extraction accuracy, $\bar{I}_{drain}$ should be chosen as large as possible but should not bring a temperature problem. We increase the $\bar{I}_{drain}$ to 5 A, then $\Delta\bar{I}_{drain}$ is set at 50 mA, and $\overline{V_B} - 2\overline{V}_{F\_D2}$ is tested at 5 A $\bar{I}_{drain}$ and set at 1.4 V, other variables are the same as above. Then, the total absolute error ΔR_{dson} should be updated by

$$\Delta R_{dson} = \sqrt{(0.012/5 + 0.07/25)^2 + (16.6\text{m}/5)^2} \approx 6.2\ m\Omega$$

Therefore, extraction accuracy of dynamic R_{dson} should be

$$\varepsilon = [1 - 6.2m/(1.4/5)] \cdot 100\% \approx 97.8\%.$$

Therefore, the larger I_{drain}, the better extraction accuracy of dynamic R_{dson}. When the dynamic R_{dson} is measured under more severe conditions, the dynamic R_{dson} will be larger, then the V_B will be larger, and the calculated extraction accuracy will be higher.

V. CONCLUSION

A novel DDI method for extracting the dynamic R_{dson} of AlGaN/GaN HEMT power devices has been proposed and an extracting accuracy of 97.8% is achieved with f_s up to 1 MHz with a V_{ds_off} that is under 600 V. The role of freewheeling diodes and parasitic capacitance of devices, and the relationships between dynamic R_{dson} and V_{ds_off}, f_s and D are investigated, then, 100 ns response time can be obtained by employing low-parasitic-capacitance devices. In

addition, extraction accuracy of dynamic R_{dson} in the test circuit can be further improved by employing a high-precision constant current source, or testing in a larger I_{drain}. This measurement technique can also be used on the Si-MOSFET, SiC-MOSFET and other FETs to extract their R_{dson} even in the conditions of high-voltage and high-frequency.

REFERENCES

[1] J. A. del Alamo and J. Joh, "GaN HEMT reliability," *Microelectron. Rel.*, vol. 49, nos. 9–11, pp. 1200–1206, Sep./Nov. 2009. doi: 10.1016/j.microrel.2009.07.003.

[2] U. K. Mishra, P. Parikh, and Y.-F. Wu, "AlGaN/GaN HEMTs-An overview of device operation and applications," *Proc. IEEE*, vol. 90, no. 6, pp. 1022–1031, Jun. 2002. doi: 10.1109/JPROC.2002.1021567.

[3] O. Ambacher *et al.*, "Two dimensional electron gases induced by spontaneous and piezoelectric polarization in undoped and doped AlGaN/GaN heterostructures," *J. Appl. Phys.*, vol. 87, no. 1, pp. 334–344, Jan. 2000. doi: 10.1063/1.371866.

[4] A. M. Wells, M. J. Uren, R. S. Balmer, K. P. Hilton, T. Martin, and M. Missous, "Direct demonstration of the 'virtual gate' mechanism for current collapse in AlGaN/GaN HFETs," *Solid-State Electron.*, vol. 49, no. 2, pp. 279–282, Oct. 2004. doi: 10.1016/j.sse.2004.10.003.

[5] R. J. Trew, D. S. Green, and J. B. Shealy, "AlGaN/GaN HFET reliability," *IEEE Microw. Mag.*, vol. 10, no. 4, pp. 116–127, Jun. 2009. doi: 10.1109/MMM.2009.932286.

[6] H. Wang, C. Liu, Q. Jiang, Z. Tang, and K. J. Chen, "Dynamic performance of AlN-passivated AlGaN/GaN MIS-high electron mobility transistors under hard switching operation," *IEEE Electron Device Lett.*, vol. 36, no. 8, pp. 760–762, Aug. 2015. doi: 10.1109/LED.2015.2450695.

[7] J. Böcker, C. Kuring, M. Tannhäuser, and S. Dieckerhoff, "Ron increase in GaN HEMTs—Temperature or trapping effects," in *Proc. IEEE ECCE*, Cincinnati, OH, USA, Oct. 2017, pp. 1975–1981. doi: 10.1109/ECCE.2017.8096398.

[8] D. Jin and J. A. del Alamo, "Mechanisms responsible for dynamic ON-resistance in GaN high-voltage HEMTs," in *Proc. IEEE 24th Int. Symp. ISPSD*, Jun. 2012, pp. 333–336. doi: 10.1109/ISPSD.2012.6229089.

[9] J. M. Lei, D. J. Chen, and Z. L. Xie, "High frequency and high voltage dynamic on-resistance extraction circuit and extraction method for AlGaN/GaN HEMT device," Chinese Patent CN 201 810 524 516.4, May 28, 2018.

[10] B. Lu, T. Palacios, D. Risbud, S. Bahl, and D. I. Anderson, "Extraction of dynamic on-resistance in GaN transistors: Under soft- and hard-switching conditions," in *Proc. IEEE CSICS*, Nov. 2011, pp. 1–4. doi: 10.1109/CSICS.2011.6062461.

[11] N. Badawi, O. Hilt, E. Behat-Treidel, J. Böcker, J. Würfl, and S. Dieckerhoff, "Investigation of the dynamic on-state resistance of 600V normally-off and normally-on GaN HEMTs," *IEEE Trans. Ind. Appl.*, vol. 52, no. 6, pp. 4955–4964, Nov./Dec. 2016. doi: 10.1109/TIA.2016.2585564.

[12] J. Everts *et al.*, "A hard switching VIENNA boost converter for characterization of AlGaN/GaN/AlGaN power DHFETs," in *Proc. Int. Exhibit. Conf. Power Electron. Intell. Motion Power Qual. (PCIM)*, 2010, pp. 309–314. [Online]. Available: https://lirias.kuleuven.be/handle/123456789/268625

[13] Y. F. Wu, M. Jacob-Mitos, M. L. Moore, and S. Heikman, "A 97.8% efficient GaN HEMT boost converter with 300-W output power at 1 MHz," *IEEE Electron Device Lett.*, vol. 29, no. 8, pp. 824–826, Aug. 2008. doi: 10.1109/LED.2008.2000921.

[14] R. Gelagaev, P. Jacqmaer, J. Everts, and J. Driesen, "A novel voltage clamp circuit for the measurement of transistor dynamic on-resistance," in *Proc. IEEE Int. I2MTC*, May 2012, pp. 111–116. doi: 10.1109/I2MTC.2012.6229275.

[15] R. Gelagaev, P. Jacqmaer, and J. Driesen, "A fast voltage clamp circuit for the accurate measurement of the dynamic ON-resistance of power transistors," *IEEE Trans. Ind. Electron.*, vol. 62, no. 2, pp. 1241–1250, Feb. 2015. doi: 10.1109/TIE.2014.2349876.

[16] U. Focken, M. Lange, K. Mönnich, H.-P. Waldl, H. G. Beyer, and A. Luig, "Short-term prediction of the aggregated power output of wind farms—A statistical analysis of the reduction of the prediction error by spatial smoothing effects," *J. Wind Eng. Ind. Aerodyn.*, vol. 90, no. 3, pp. 231–246, Mar. 2002. doi: 10.1016/S0167-6105(01)00222-7.

[17] C. Bo, Z. Yang, L. Wang, and H. Chen, "A comparison of tolerance analysis models for assembly," *Int. J. Adv. Manuf. Technol.*, vol. 68, nos. 1–4, pp. 739–754, Sep. 2013. doi: 10.1007/s00170-013-4795-2.

[18] W. H. Greenwood and K. W. Chase, "Root sum squares tolerance analysis with nonlinear problems," *ASME. J. Eng. Ind.*, vol. 112, no. 4, pp. 382–384, Nov. 1990. doi: 10.1115/1.2899604.